Manuscript prepared for Nonlin. Processes Geophys.
with version 2014/05/15 6.81 Copernicus papers of the LaTeX class copernicus.cls.
Date: 28 June 2014

An early warning indicator for blocking events

Fiona R. van der Burgt[1], **A. Tantet**[1], **and H.A. Dijkstra**[1]

[1]Institute for Marine and Atmospheric Research, Utrecht University, Utrecht, The Netherlands

Correspondence to: F. R. van der Burgt (F.R.vanderBurgt@students.uu.nl)

Abstract.

The formation of a persistent high pressure cell in the mid-latitudes that blocks the westerly flow is called a blocking event. Such events have a high impact on the general weather in these areas. In one of the theories of the transitions between zonal and blocked flow, the interaction of the atmospheric jet with the orography causes multiple equilibria in the mean state of the atmospheric flow. The main aim of this study is to develop an early warning indicator for such a transition. A new method is developed to define regime switches in the highly dimensional climate system. A barotropic vorticity model of the Northern Hemisphere, truncated at the 21st wavenumber and with realistic topography and forcing is used to simulate transitions into a blocked state of the atmosphere. The projection of all the states of the model into the plane defined by the leading Empirical Orthogonal Functions (EOF) of the streamfunction shows two attracting regions; the zonal and the blocked state of the model. The evolution in time shows preferred directions of movement in this phase-space. A complex network is built where the attracting regions are represented by highly connected nodes. We show that it is possible to identify two persistent atmospheric regimes by using a community detection algorithm on this network. Probabilities to make the transition to the blocked regime are calculated from the trajectories on this plane. From these probabilities, an early warning indicator for the transition into the blocked state can be derived that gives the most reliable results on longer timescales. Finally, a physical mechanism for the transitions to the blocked regime is found from the energetics of the system. As the system gets barotropically unstable, perturbations are enhanced by the increasing Reynolds stresses. The coupling of the flow with the topography gives rise to a loss of energy of the zonal flow towards meandering modes.

1 Introduction

Blocking episodes are one of the most important weather aspects of the midlatitudes. A high pressure system is formed that blocks the mean westerly flow and strongly affects the weather over Europe, especially in winter, by advecting cold air from Siberia into North-Western Europe, causing cold, winterly conditions.

Scientific effort has been put in the definition of a blocking event, both in spatial distribution and temporal duration. In the Northern Hemisphere, there are two preferred regions for blocking; the Atlantic and Pacific region. The first definition of blocking events was given by Rex (1950a, b) as a change in the midlatitude flow which should persist for at least 10 days. Later, other definitions where suggested by Lejenäs and Ø kland (1983) and Tibaldi and Molteni (1990), considering the zonal mean geopotential height at different latitudes. Pelly and Hoskins (2003) investigated potential temperature (θ) on the dynamical tropopause, defined by the surface that has a potential vorticity of 2 potential vorticity units (PVU). In general, the polar regions are characterised by low values of θ on the PV=2 field, whereas the tropics are characterised by high θ. This normally negative meridional gradient becomes positive during a blocking episode, when breaking of waves cuts off tropical air with high potential temperature from the tropical region.

Other studies consider the link with dominant large scale atmospheric patterns such as the North Atlantic Oscillation (NAO) and the Pacific North American (PNA) pattern. Croci-Maspoli et al. (2007); Woollings et al. (2008); Thompson and Wallace (2001) showed that low index conditions of the Northern Annular Mode (NAM) are suggestive of blocking and that there is a strong anti-correlation between blocking and the phase of the NAO (PNA). Prediction of the formation of blocking highs with models remains however problematic, as models have difficulties with the onset of blocking (Tibaldi and Molteni (1990); Mauritsen and Källén (2004)).

A dynamical mechanism that might explain the existence of blocking highs was presented by Charney and DeVore (1979). This relatively simple model of zonal flow through a channel with topography gives some insight in the dynamical processes responsible for blocking-like behaviour. The paper finds mathematical evidence of a zonal mean flow of the atmosphere with multiple equilibria. One state is associated with strong zonal winds, whereas the other state has weak zonal winds and more meandering of the flow. The existence of multiple equilibria is due to an interaction of the flow with the topography. The transitions between the states are forced by small scale instabilities.

Of course, the model by Charney and DeVore (1979) is very simplistic, but also in more complex models signs of regimes in the flow pattern are found. The persistence in some regions in phase space suggests the presence of a complex, multidimensional attractor. Dependent on the strength of the forcing or the dissipation, a barotropic model that is truncated at a specific wavenumber can behave in different patterns. Furthermore, the interactions between different waves lead to additional solutions (Legras and Ghil (1985)). Itoh and Kimoto (1996) showed that such models have oscillatory modes between those attractors. Even when stochastic forcing is applied, the transits of the model will follow the ruins of the now unstable attractor. A study by Jin and Ghil (1990) gave some insight in the dynamics of intraseasonal oscillations in the Northern hemisphere by considering bifurcations in a barotropic potential vorticity model due to interactions of waves with the mean flow and the influence of topography. Crommelin (2003) suggests that the regime transitions between a blocked and zonal state in a barotropic model truncated at the 21st wavenumber might be the remnants of a homoclinic orbit in this highly dimensional system.

The view on the climate system as a system that can shift between two different equilibrium states gives rise to the question whether we can predict the transition just before it happens (Lenton (2011)). A traditional method that gives an early warning of a sudden transition is the use of the critical slow down of the system when it gets close to its bifurcation point (Scheffer et al. (2009)). However, in such high dimensional models it is too simplistic to reduce the topology of the system to one or more stable fixed points. To detect the mode or dimension where the critical slowdown will take place is absolutely not trivial and one should think of other methods to find an indicator of the transition. Recently, different studies showed that complex networks can reveal information on nearby sudden changes in the mean state of the system (VanderMheen2013, Viebahn and Dijkstra (2013)). By looking at changes in the topology of the network, an early warning indicator for a transition in the mean state of the system can be developed.

This paper discusses a method to define regimes or 'attracting points' in the multidimensional climate system as persistent regions of the phase space. First, the states of the model are projected in the phase-space that is defined by the Empirical Orthogonal Funtions (EOFs) and in this phase space, a complex network is defined. The communities in this network reveil attracting points in phase space. The method is applied to a barotropic model with Northern Hemisphere topography, forced under winterly conditions. A blocked and zonal regime are defined in section 2. With these definitions, it is possible to calculate the probabilities of reaching the blocked state and evidence of an early warning indicator for the transition to a blocked state is found in section 3. In section 4 the physical mechanism explaining the transition is explained with a low order barotropic model.

2 Regimes in the T21-barotropic model

Transitions between zonal and blocked state of the atmosphere are investigated in the context of a T21 barotropic model of the Northern Hemisphere. This model was also used by Selten (1995) and Crommelin (2003). In this section first the model characteristics are described and then continues with a new method to define regimes in such a high dimensional system.

2.1 The T21-barotropic model

The dimensionless equation of the model, expressed in terms of the streamfunction ψ and the relative vorticity $\zeta = \nabla^2\psi$, is given by:

$$\frac{\partial \zeta}{\partial t} = \mathcal{J}(\psi, \zeta + f + h) - k_1\zeta + k_2\Delta^3\zeta + \zeta^*. \quad (1)$$

$\mathcal{J}$ denotes the Jacobian operator, f the Coriolis parameter, h a prescribed orography, k_1 the Ekman damping coefficient, k_2 the coefficient of scale-selective damping and ζ^* a constant vorticity forcing. The streamfunction is expanded in series of spherical harmonics $Y_{m,n}(\lambda, \mu)$. In this case the modes are triangularly truncated at wavenumber 21:

$$\psi(\lambda, \mu, t) = \sum_{n=1}^{21} \sum_{\substack{m=-n \\ m+n=odd}}^{+n} \psi_{m,n}(t) Y_{m,n}.(\lambda, \mu) \quad (2)$$

Boundary conditions are applied as the model is hemispheric. Currents crossing the equator are not allowed. This leaves the restriction of $m + n$ being odd, and therefore 231 degrees of freedom in the model. The orography was also truncated at wavenumber 21. The forcing ζ^* was used as in Selten (1995), calculated from a climatology from ECMWF Reanalysis in order for this climatology to be a fixed point of the barotropic vorticity equation:

$$\zeta^* = \mathcal{J}(\psi_{cl}, \zeta_{cl} + f + h) - k_1\zeta_{cl} + k_2\Delta^3\zeta_{cl} + \overline{\mathcal{J}(\psi', \zeta')}, \quad (3)$$

with ψ_{cl}, ζ_{cl} climatological winter mean state of 10 winters and $\overline{\mathcal{J}(\psi', \zeta')}$ the time average of the Jacobian of deviations of the 10-day running mean of this climatological mean

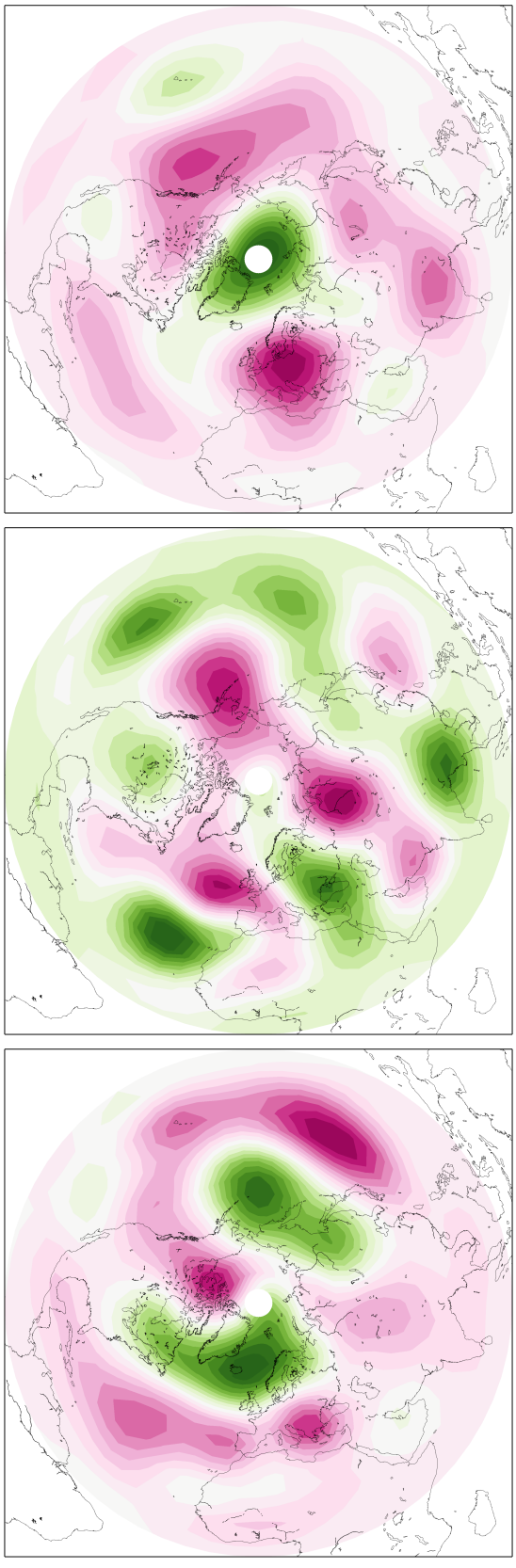

Figure 1. First three EOFs of the T21 barotropic model. EOF 1, 21.0% of the variance, EOF 1, 8.3% of the variance, EOF 3, 6.9% of the variance.

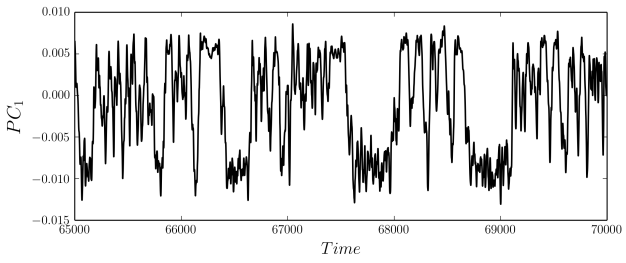

Figure 2. Part of the PC1 time series. Low values of PC1 are associated with blocking-like states of the model. The irregularity of the time series makes it however difficult to make a proper definition of the blocked states directly from this PC.

ψ', ζ'. After a run, the observed transient eddy forcing in ζ^* was replaced by the model transient eddy forcing that was determined from that run. This was done a second and third time, until the model mean state and variability where close enough to the observations.

A 200 year run was done under constant winterly conditions in the forcing ζ^*. The daily output of the model generated a dataset of 73,000 datapoints. An analysis of the (in total 231) EOFs of the streamfunction shows that the variability is spread in many different EOFs. The first three EOFs explain in total 41.7% of the variability, see figure 1. The first EOF (21.0%) resembles the pattern of the Arctic Oscillation (AO) and is associated with the strength of the polar vortex. It looks like the mean state of the model (Selten (1995)). The second EOF (8.3%) shows anomalies over Western Europe. The third EOF (6.9%) resembles the pattern of the North Atlantic Oscillation (NAO), as it shows a dipole-like pattern over the Atlantic and Pacific region.

The principal component (PC) of the first EOF is partially plotted in figure 2. In general the evolution of the time series looks very irregular, but some bimodality can be distinguished. High values of this mode indicate the zonal state, low values are associated with blocking-like periods. Crommelin (2003) already showed that the projection of all the states of the system onto the PC1-PC3 plane reveals interesting behaviour of the system. It appears that the 3rd EOF is associated with the transitions between the blocked and zonal state. The 2nd PC is not in such a way related to the transitions, and is therefore left out of scope. When all the states of the system are projected onto the PC1-PC3 plane, a figure of the density of states (DOS) is formed, see figure 3. The two maxima that are found in this DOS are associated with the blocked (low PC1 values) and zonal (high PC1 values) regimes. The light blue region around the first maximum with relatively low PC3 values shows the main 'pathway' that trajectories take when they leave the zonal regime. From these results Crommelin (2003) sketched a simplified picture of the dynamics of the system; the positive values of PC1 correspond to a weak polar vortex (negative AO phase). Via a positive NAO phase (negative PC3) the system devel-

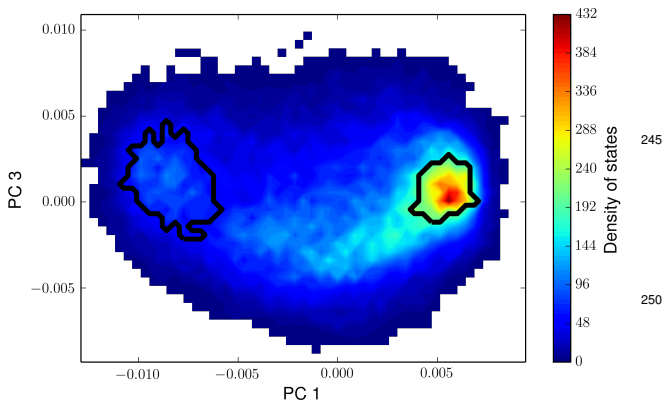

Figure 3. Colors: projection of the timeseries in the discretised PC1-PC3 space with a resolution of 42x53 grid cells. Red colours mean high density of states. Black contours: the zonal and blocked community, defined by the highest 50% of the page ranks of the two communities found from the time lag network with lag 13 (see figure 4).

ops into a state of strong polar vortex, the blocked state. The transition back to zonal is associated with a negative NAO phase.

It would be interesting, and in terms of weather prediction useful, to be able to make a prediction on the evolution of the system towards a blocked state. To be able to do so, it is important to have a good definition of the blocked and zonal states in the phase space to indicate the exact moment of departure from or arrival in one of the two regimes. Furthermore, a separation has to be made between the trajectories that leave the zonal state and then turn back, and the ones that indeed make the regime transition.

2.2 Complex networks and flow regimes

To define the two attracting regimes, we made use of a complex network. The network was constructed in the PC1-PC3 plane, that was discretised in 53×42 grid cells. Every grid cell represents a node in the network, so the adjacency matrix A has dimension 2226×2226. An observation at time i, n_i is said to be connected to an observation at a certain lag in the future, n_{i+lag}. The projection of state n_i and state n_{i+lag} in the grid cells in the PC-plane results in a link between those two cells. This was done for all the states of the model to construct an adjacency matrix A that is weighted and directed. Multiple observations can project into one box in the phase space and a link will always have a certain direction. This direction indicates the future development of the model in phase-space and multiple links will therefore indicate a preferred direction of movement.

We call this network the time-lag network. It has $53x26 = 2226$ nodes and $73000-lag$ links. The degree map of the network looks similar to the DOS-figure above, as the amount of links is almost the same as the amount of states. The zonal region will still be a region of high degree, as multiple states tend to go there within a certain lag. The points that are attracting in phase space, will look in the network as highly connected nodes. The separation between those highly connected nodes can be interpreted as a separation between different states of the model. We are therefore interested in the community structures that can be found in this network; a division of the network in subgroups that are in itself highly connected, but the connections between those subgroups are sparse (Newman and Girvan (2008)).

To calculate the community structures in the network, the Infomap software, developed by Rosvall and Bergstrom (2008, 2011) was used. This software uses a random walker as a proxy for real network flow. The shortest possible description of this random walker on multiple levels gives the best hierarchical clustering of the network. The importance of a community in a network can be measured by the pagerank of all the nodes in that community (Brin and Page (1998)). The pagerank is the probability to end up on the node for a random walker when the stationary distribution is calculated.

For different lags, a network was constructed and with the Infomap software the communities where calculated. This resulted in some cases where there where some isolated nodes that didn't belong to any community. Those nodes, with a pagerank lower than 1%, where expected not to be representative for the average behaviour of the system and were therefore removed.

The community structure of the network is sensitive for the choice of the lag. Also the importance of communities changes with changing lag. Figure 4 shows the community structure for lag 3 and lag 13. The results reveal properties of the system on different timescales. For short lags (1-5 days), many communities with relatively low page ranks are found, whereas for longer lags ($\geq$ 13 days), only two communities with high page ranks remain, see figure 4. Those two communities represent a separation in phase space between zonal-like and blocked-like, with the zonal community having a much higher pagerank than the blocked community.

These results can be explained from the fact that on short timescales, the system has no preferred direction of movement. States move only small distances in phase-space. On long timescales however, states are attracted to one of the two attractors in the DOS: either the zonal or the blocked state. With increasing lags, the number of communities slowly decreases. For timelags of 7 days and more, the zonal and blocked communities start to emerge, apart from a few 'transition' communities.

From the communities in the time-lag network with lag-13, the definition of the blocked and zonal regime was made, as this was the shortest lag were two communities were found. To find the most important nodes in each community, the maximum pagerank of each community was determined.The regimes where said to be all the nodes that have a pagerank of $\geq 50\%$ from the maximum pagerank found

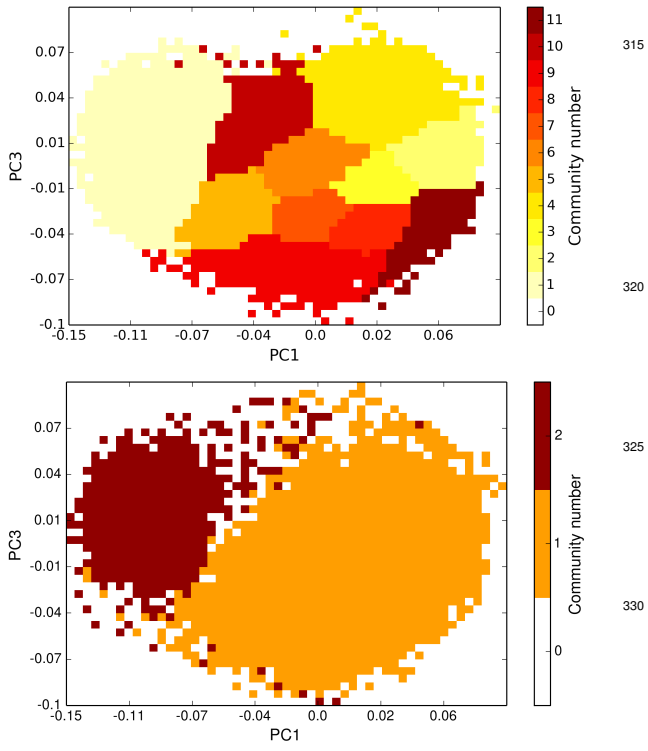

Figure 4. Communities found in the time-lag network for lags 3 (upper) and 13 (lower). Colors indicate the different communities. Communities with a low number have the highest page rank. White means no community, or a community with a pagerank lower than 1%. For lag 3 many different communities are found, whereas for lag 13 only 2 communities remain, that are associated with the zonal (orange) and blocked (red) regime.

in that community. So if the maximum pagerank found in a community is 0.8, than all the nodes that have a pagerank ≥ 0.4 define the regime. The few nodes that were member of the regime by this definition, but were isolated from the rest were removed. The location of the regimes is indicated in figure 3 by the black solid curves.

3 The early warning indicator

3.1 Trajectories

The full time series of 73,000 states can be split up in a dataset of trajectories. Trajectories start when they leave, and end when they enter one of the two regimes as indicated in figure 3. Therefore, there are four different types of trajectories: going from zonal to blocked (ZB), from zonal to zonal (ZZ), from blocked to zonal (BZ) and from blocked to blocked (BB). It appears that the ZZ-paths can be particularly slow (up to a maximum of 900 days), whereas the average duration of a transition from zonal to blocked takes about 60 days. For every grid cell in the discretised phase space all the ZB trajectories that pass through that cell can be counted and divided by the total amount of states that projects in that cell. In this way, a probability distribution of coming from zonal and going to blocked is found:

$$P_{ZB} = \frac{\sum_{n \in ZB} n_i}{\sum n_i}, \tag{4}$$

where n are all the states, and $n \in$ ZB are all the states that belong to trajectories from zonal to blocked. The resulting transition probability figure is shown in the upper frame of figure 5. The preferred region in phase space for the ZB trajectories is the region of low values of PC3. Red colours indicate that almost all the trajectories at that point belong to the come from zonal and go to the blocked region. However, as is shown in the DOS in figure 3, only a small amount of trajectories gets into this region of phase-space.

In the same way, a transition probability figure can be made for the transition into the blocked state from anywhere in phase space, within a certain time. This gives the probability of making the transition into the blocked state within a certain time threshold, τ_c:

$$P_{\tau_c} = \frac{\sum_{n \in ZB(\tau_c), BB(\tau_c)} n_i}{\sum n_i}. \tag{5}$$

$\mathrm{ZB}(\tau_c)$ and $\mathrm{BB}(\tau_c)$ are all the states that will make the transition to the blocked regime within the time τ_c. This transition probability for $\tau_c = 50$ is shown in the lower frame of figure 5.

3.2 Quality factor

The transition probability figures give an indication for the evolution of the system. The goal is to find an early warning indicator for the transition to the blocked state. This indicator should give a warning when the system shifts towards a blocked state, but not when the system turns back to the zonal regime. An optimal indicator doesn't miss any alarm, nor does it give any false alarms.

By following a trajectory in time, the probability of reaching the blocked state changes. It might reach at a certain moment a location in phase space where this probability exceeds a set warning threshold, p_c, where p_c can range between 0 and 1. This threshold will be the indicator: at the moment that p_c is exceeded, a warning is given. This warning tells that the system will in the future shift into the blocked state. The question is however how far in the future this will be. This is defined by the time threshold, τ_c, the maximum time that is allowed for the transition to actually happen.

The trajectories were divided into two sets of zonal-to-zonal and zonal-to-blocked trajectories over which the indicator was tested. When the indicator gives an alarm in a trajectory going from zonal to zonal, this will be a false alarm. Alarms that are too early (the alarm is given prior to the time threshold τ_c), are also counted as a false alarm. The missed

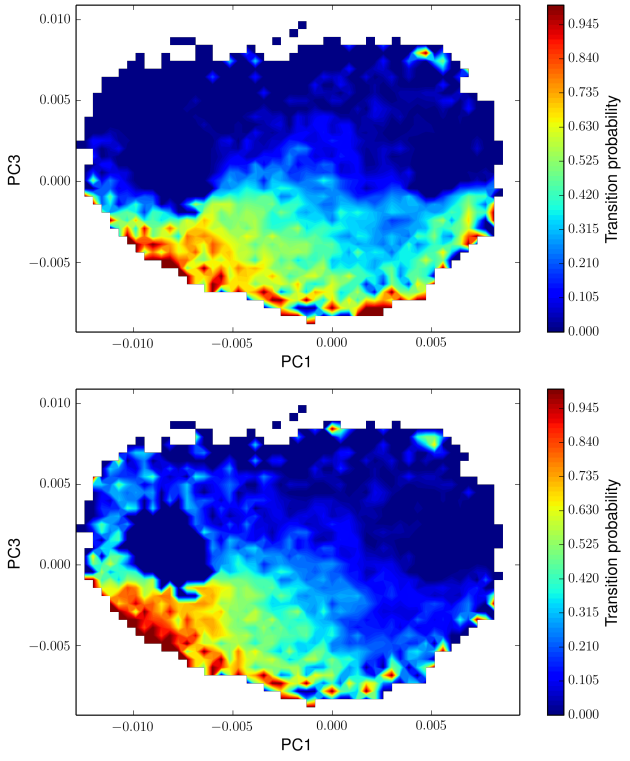

Figure 5. Probabilities of reaching the blocked state at any time when coming from zonal state (upper) and and when coming from anywhere in phase space (lower). Both figures are normalised to the total amount of all possible trajectories.

alarms are the trajectories from zonal to blocked that do not reach the warning threshold.

We can now define a quality factor Q that quantifies the quality of the early warning indicator.

$$Q = (1 - M)(1 - F). \tag{6}$$

Here, M is the fraction of the amount of missed alarms over the amount of ZB trajectories, and F is the fraction of the amount of false alarms over the total amount of trajectories. F and M both depend on two parameters: the indicator p_c, and the time threshold τ_c.

In figure 6, Q is plotted against τ_c for different values of p_c. In general, a low p_c will result in a low number of missed alarms, but a high number of false alarms. A long prediction threshold on the other hand reduces the chance on an alarm that is too early and therefore reduce the amount of false warnings.

It might seem counterintuitive that it is easier to predict the system on longer timescales than on shorter. This has however to do with the cumulative effect that the system will reach the blocked state *within* the prediction threshold. Predictions on longer timescales are therefore less accurate at the moment when the system will reach the other

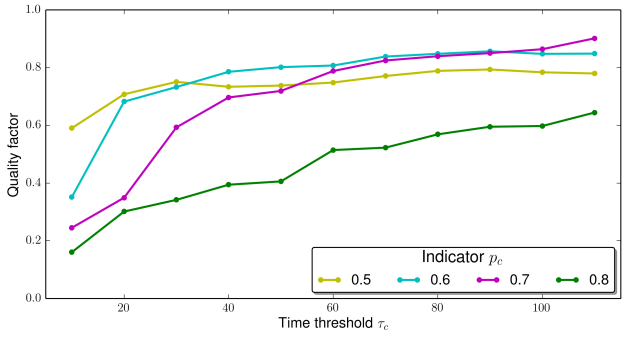

Figure 6. Quality factor of the early warning indicator versus the prediction threshold for four different warning thresholds p_c.

regime than predictions on shorter timescale. Also, the use of a longer time threshold will result in a better defined pathway of the transition into the blocked state in phase space. In conclusion, the indicator detects whether the system is in a favourable state to make the transition towards the blocked state.

The best results are obtained for $p_c = 0.6$ and $\tau_c > 40$ days. For $\tau_c = 40$ days, the amount of false alarms is still 18% and the amount of missed alarms is 4%, but for $\tau_c = 110$ days, this has reduced to 14% and 1% respectively. An even better result in terms of less false alarms can be obtained by taking $p_c = 0.7$, $\tau_c = 110$ days, with 7% false alarms and 4% missed alarms.

4 Physics of the transition

So far a statistical method is found to describe the transition into the blocked state, yet the physical mechanism underlying the transition is not investigated. It would be interesting to link the indicator (the probability to go to the blocked state) to a real physical quantity. To be able to do so, the simple six mode model derived by Charney and DeVore (1979) is investigated. With the help of the results from this low order model, the T21-model is considered again.

4.1 The low order model

This model describes a homogeneous β-plane atmosphere with a free surface height and with an idealised geometry in a zonal channel of width πbL and length $2\pi L$, where $b = 0.5$. Since the motions are large scale, they are quasi-geostrophic and governed by conservation of potential vorticity. This gives an equation for the nondimensionalised streamfunction ψ:

$$\frac{\partial \nabla^2 \psi}{\partial t} + \mathcal{J}(\psi, \nabla^2 \psi + \beta\psi + \gamma h) + C\nabla^2(\psi - \psi^*) = 0 \tag{7}$$

All the parameters in this equation are nondimensional. Length x and y was scaled with L, time with $1/f_0$, the vorticity with f_0 and the topography with H. $\beta = \beta_0 L / f_0$ and

$C = k/f_0$, where k is a measure of the Ekman damping. ψ^* is a prescribed function of the forcing. The Jacobian operator $\mathcal{J}$ operates on the variables a and b as follows:

$$\mathcal{J}(a,b) = \frac{\partial a}{\partial x}\frac{\partial b}{\partial y} - \frac{\partial b}{\partial x}\frac{\partial a}{\partial y}$$

The problem has to be simplified further, by expanding ψ and ψ^* in orthonormal eigenfunctions of the Laplace operator with boundary conditions provided by the channel. Those are given by:

$$\phi_{0,m}(y) = \sqrt{2}\cos\frac{my}{b} \tag{8a}$$

$$\phi_{n,m}(x,y) = \sqrt{2}e^{inx}\sin\frac{my}{b} \tag{8b}$$

For $n = 0, 1$ and $m = 1, 2$.

It is now possible to expand the stream function ψ, the topography h and the forcing field ψ^* in these eigenfunctions, and to substitute them into equation 7. Topography and forcing are chosen as

$$h(x,y) = \cos x \sin\frac{y}{b}; \quad \psi^*(x,y) = \Phi(y) \tag{9}$$

With $\Phi(y)$ a fixed function.

The system is furthermore simplified by only taking the modes $n = -1, 0, 1$ and $m = 0, 2$. With:

$$x_1 = \frac{1}{b}\psi_{0,1}; \quad x_4 = \frac{1}{b}\psi_{0,2}$$

$$x_2 = \frac{1}{\sqrt{2}b}(\psi_{1,1} + \psi_{-1,1}); \quad x_5 = \frac{1}{\sqrt{2}b}(\psi_{1,2} + \psi_{-1,2})$$

$$x_3 = \frac{i}{\sqrt{2}b}(\psi_{1,1} - \psi_{-1,1}); \quad x_6 = \frac{i}{\sqrt{2}b}(\psi_{1,2} - \psi_{-1,2})$$

and $x_4^* = r x_1^*$, six projected equations are found for x_n with $n = 1, .., 6$ (for further details Crommelin et al. (2004)).

$$\frac{dx_1}{dt} = \tilde{\gamma_1} x_3 - C(x_1 - x_1^*) \tag{11a}$$

$$\frac{dx_2}{dt} = -(\alpha_1 x_1 - \beta_1)x_3 - C x_2 - \delta_1 x_4 x_6 \tag{11b}$$

$$\frac{dx_3}{dt} = (\alpha_1 x_1 - \beta_1)x_2 - \gamma_1 x_1 - C x_3 + \delta_1 x_4 x_5 \tag{11c}$$

$$\frac{dx_4}{dt} = \tilde{\gamma_2} x_6 - C(x_4 - x_4^*) + \epsilon(x_2 x_6 - x_3 x_5) \tag{11d}$$

$$\frac{dx_5}{dt} = -(\alpha_2 x_1 - \beta_2)x_6 - C x_5 - \delta_2 x_4 x_3 \tag{11e}$$

$$\frac{dx_6}{dt} = (\alpha_2 x_1 - \beta_2)x_5 - \gamma_2 x_4 - C x_6 + \delta_2 x_4 x_2 \tag{11f}$$

Where terms with α reflect the advection of modes by the zonal flow, with β the advection of planetary vorticity and γ the effect of topography. δ and ϵ reflect the nonlinear interactions between the different modes.

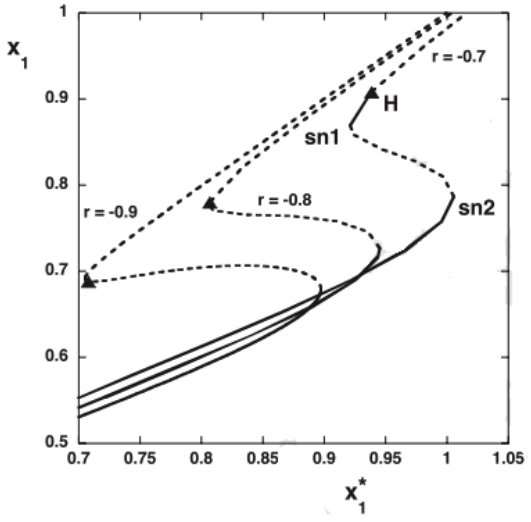

Figure 7. Bifurcation diagram for states of the first mode x_1 versus increasing forcing parameter x_1^*. Topographic amplitude $\gamma = 0.2$. An decrease in the forcing parameter r results in a shift of the Hopf bifurcation (triangle) towards the second saddle node. Figure from Dijkstra (2013).

$$\alpha_m = \frac{8\sqrt{2}}{\pi}\frac{m^2}{4m^2-1}\frac{b^2+m^2-1}{b^2+m^2}; \quad \beta_m = \frac{\beta b^2}{b^2+m^2}$$

$$\tilde{\gamma_m} = \gamma\frac{4m^2}{4m^2-1}\frac{\sqrt{2}b}{\pi}; \quad \gamma_m = \gamma\frac{4m}{4m^2-1}\frac{\sqrt{2}b}{\pi(b^2+m^2)}$$

$$\delta_m = \frac{64\sqrt{2}}{15\pi}\frac{b^2-m^2+1}{b^2+m^2}; \quad \epsilon = \frac{16\sqrt{2}}{5\pi}$$

Finally, ψ can be written as:

$$\psi = b x_1\sqrt{2}\cos\frac{y}{b} + 2b(x_2\cos x + x_3\sin x)\sin\frac{y}{b}$$
$$+ b x_4\sqrt{2}\cos\frac{2y}{b} + 2b(x_5\cos x + x_6\sin x)\sin\frac{2y}{b}$$
$$= \psi_{01} + \psi_{11} + \psi_{02} + \psi_{12} \tag{13}$$

4.2 Multiple equilibria

As was shown by Charney and DeVore (1979), the first three modes of this low order model already have multiple steady equilibria. Due to the presence of the topography the system has a stable zonal state, a stable blocked state and between these two states an unstable branch of solutions. The zonal flow is characterised by a strong zonal wave component (upper branch), whereas the blocked flow has less high wind speeds (lower branch). In the nondissipative case $C = 0$, it can be shown that exponential growth of perturbations of the

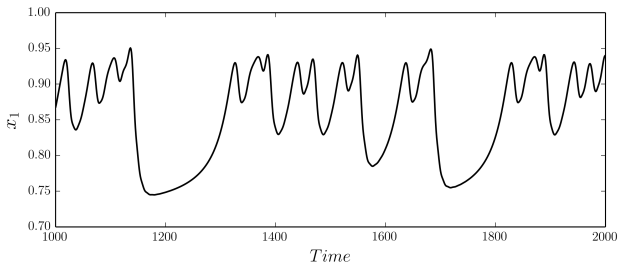

Figure 8. Timeseries of the first mode of the low order model. High values of the first mode indicate the zonal state.

modes can occur when the topography height γ is non zero. This is called topographic instability.

The bifurcation diagram of the system with $\gamma = 0.2$ and for different values of the forcing parameter r is shown in figure 7. With this amplitude of the topography, the regime of the multiple equilibria shifts to quite realistic values of wind speed and forcing (Crommelin et al. (2004)). The forcing of the fourth mode is coupled to the forcing of the first mode with parameter r: $x_4^* = rx_1^*$, ($r < 0$). An increase of r (r gets less negative) will finally lead to the vanishing of the multiple equilibria.

The triangle on the upper branch marks a Hopf bifurcation and is associated with barotropic instability. For a certain strength of the zonal forcing, the meridional gradients of wind speed in the jet become too large. The zonal flow loses it's stability and a stable oscillatory wave mode is created.

An increase of the coupling parameter r will also result in a shift of the Hopf-bifurcation towards the second saddle node, as in this case the fourth mode -the only zonal mode that can get barotropic unstable- is stronger forced. For a certain value of r, the bifurcations will overlap, forming a so-called fold-Hopf-bifurcation with codimension two. At this point, one eigenvalue of the system is exactly zero, whereas two others will be purely imaginary. Fold-Hopf-bifurcations can give rise to other bifurcations, such as homoclinic orbits (Crommelin et al. (2004)). Homoclinic orbits connect saddle equilibria to themselves. This type of connection can possibly lead to chaotic behaviour (Kuznetsov et al. (2004); de Swart (1989)) which could reduce the predictability of the model.

4.3 Physical properties in the low order model

A run of the model was done as in Crommelin et al. (2004) with $(r, x_1^*) = (-0.801, 0.95)$. With this choice of parameters spontaneous transitions occur from one branch to another due to the presence of the fold-Hopf bifurcation. In physical terms this means that the zonal flow gets barotropically unstable and the amplitude of the first mode is reduced. So far, no chaotic behaviour could be found in a small range of (r, x_1^*) around these values. The time series of the first mode are shown in figure 8.

The question is why the system in some cases quickly turns back towards the zonal state, whereas in other cases it seems to be captured in a state of less zonal strength. A possible candidate responsible for this kind of behaviour could be transfer of momentum from the flow to the bottom topography, the so-called form drag (Holloway (1987); Warren et al. (1996)). Depending on the shape of the topography and the strength of the zonal flow, the flow can get destabilised by presence of the bottom irregularities (Frederiksen and Frederiksen (1989); Benilov (2000); Benilov et al. (2004)). When the form drag is nonzero, it modifies the total integrated momentum of the system. However, as Frederiksen and Frederiksen (1991) suggest, topography can also act as a catalyst in the coupling between the mean state and disturbances that are for example caused by barotropic instability.

In the low order model, the form drag of the mean flow is exactly zero, due to symmetry of the topography and the flow patterns. Small perturbations on the mean flow do however interact with the topography. When the barotropic vorticity equation 7 is multiplied with the fluctuating component of the stream function ψ' and averaged in time, an equation is found for the energy of the perturbations of the mean flow:

$$\psi' \frac{\partial \zeta'}{\partial t} + \psi' \mathcal{J}(\bar{\psi} + \psi', \bar{\zeta} + \zeta' + \beta y + \gamma h) = \psi' C(\zeta^* - \bar{\zeta} - \zeta') \tag{14}$$

The first term on the left hand represents the tendency of the energy, the second term the advection, the third term is the coupling of the perturbations to the mean flow via the topography and the fourth term is the effect of the Coriolis force. The terms on the right hand side represent the forcing of the mean flow, the dissipation of energy and the Reynolds stresses.

The mean flow $\overline{\psi}$ is determined by the state the system was in before the transition set in. When $x_1 > 0.87$ the flow is defined to be in the zonal state. The threshold > 0.87 was arbitrarily chosen and the results are not sensitive to small changes in this value, as long as the zonal state is defined as a state of high values of x_1.

$$\overline{\psi} = \overline{\psi_z} = \frac{1}{n_z} \sum_{x_1 \in Z} \psi_i \tag{15}$$

With n_z the amount of states in the zonal regime. The perturbations are now defined as:

$$\psi' = \psi - \overline{\psi_z} \tag{16}$$

Note that this means that a time average of the perturbations $\overline{\psi'}$ is not necessarily zero.

When equation 14 is now time averaged, the equation for the development of turbulent kinetic energy (TKE), is found. In this equation, terms remain of $\mathcal{O}(\psi')$, as $\overline{\psi'} \neq 0$.

This equation can be integrated over the total (periodic) domain, whereby the symmetrical terms (in this case the advection terms) will drop out, and what is left is an equation for the evolution of the total TKE of the system.

$$\frac{\partial \overline{|\nabla \psi'|^2}}{\partial t} = -\bar{\psi}\overline{\mathcal{J}(\psi', \zeta')} - C\overline{\psi'\zeta'} - \mathcal{O}(\psi') \tag{17}$$

The first term represents the tendency of the TKE. On the right hand side are the Reynolds stresses, the dissipation and finally the coupling with the mean flow.

Figure 9 shows an example of the the transition from zonal to blocked flow around $t = 4470$ in the black line. In the coloured lines the associated energy budgets that contribute to the TKE integrated over the total domain are shown. The time average is taken over 5 time steps. The transition starts when the system gets out of equilibrium due to the fold Hopf bifurcation. This is physically a barotropic instability in the ψ_{02} mode. Just before the first mode reaches its maximum value after which it suddenly drops to lower values associated with the blocked state, the Reynolds stresses become strongly positive. This means that the perturbations, caused by the barotropic instability extract energy from the mean flow and grow. This is indeed seen in the strong increase in TKE. After a short while, the dissipation and the $\mathcal{O}(\psi')$ increase, causing a reduction of the TKE again. The Reynolds stresses are therefore the main driver of the transition towards a blocked state, but this doesn't explain yet why the pattern of the atmospheric flow changes so drastically.

From the coupling of the mean flow with the topography it can be shown that the transition of the system to a blocked state is associated with a transfer of energy from the zonal modes towards the meandering modes. The coupling of the perturbations of the flow with the topography causes an energy transfer from the zonal modes towards the meandering modes:

$$E_{01} = \int_0^{2\pi}\int_0^{b\pi} \psi' \mathcal{J}(\psi'_{01}, \gamma h) dy dx = -\gamma \frac{2}{3}\sqrt{2}\pi x'_1 x'_3 \tag{18a}$$

$$E_{11} = \int_0^{2\pi}\int_0^{b\pi} \psi' \mathcal{J}(\psi'_{11}, \gamma h) dy dx = \gamma \frac{2}{3}\sqrt{2}\pi x'_1 x'_3 \tag{18b}$$

$$E_{02} = \int_0^{2\pi}\int_0^{b\pi} \psi' \mathcal{J}(\psi'_{02}, \gamma h) dy dx = -\gamma \frac{16}{15}\sqrt{2}\pi x'_4 x'_6 \tag{18c}$$

$$E_{12} = \int_0^{2\pi}\int_0^{b\pi} \psi' \mathcal{J}(\psi'_{12}, \gamma h) dy dx = \gamma \frac{16}{15}\sqrt{2}\pi x'_4 x'_6 \tag{18d}$$

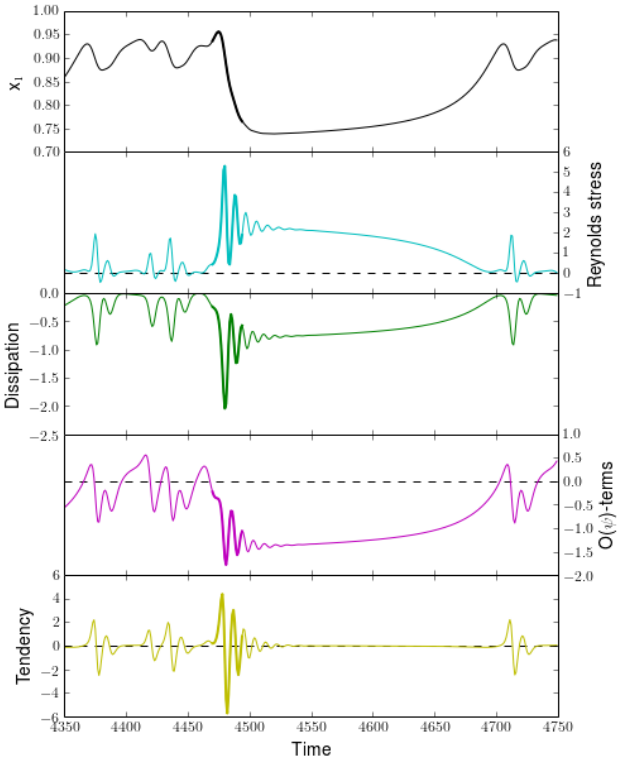

Figure 9. In the upper panel an example of the transition to the blocked state in the time series of the first mode (black line), low values of the first mode are associated with the blocked state. The transition is around $t = 4470$ and is marked by the thick line. The Reynolds stresses (blue line), the dissipation of the disturbances (green line), the grouped $\mathcal{O}(\psi')$ terms (pink line) and the tendency of the TKE (yellow line).

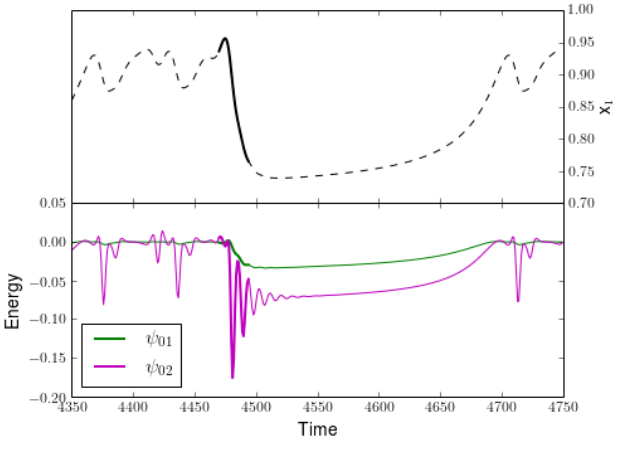

Figure 10. Time series of the first mode (black dotted line), and energy losses of the perturbations in the zonal modes. ψ'_{01} green line and ψ'_{02} in the pink line. The pink line shows the barotropic instability in this mode. The transition is marked by the thick line.

In figure 10 the energy losses of the zonal modes are plotted during the transition. The system gets out of equilibrium due to the fold Hopf bifurcation. This is physically a barotropic instability in the ψ_{02} mode. The mode gets out of phase with the topography, thereby loosing energy. At the same moment the opposite happens to the ψ_{12} mode, which gains this energy from the coupling with the topography. A similar process happens for the ψ_{01} and the ψ_{11} modes, apart from the fact that these modes do not get barotropically unstable, but get perturbed by the changes in the wavenumber-2 modes. This process pushes the system into a state of reduced zonal strength, from where it slowly turns back into the zonal state due to the zonal forcing that is applied to the system.

4.4 Physical properties in the T21-model

With the results that were found in the low order model, the T21-model can now be considered again. Due to the larger dimensions of the system it is hard to show the energy transfer between te zonal and non-zonal modes, yet it is possible to investigate the influence the Reynolds stresses. In the end, the link will be made with the indicator derived in section 3.

In general, the blocked state is in the T21 model associated with an enhanced (and reversed with respect to the zonal state) polar vortex, and anticyclonic motion over Western Europe. The Westerly winds in the midlatitudes are stronger in the zonal state and moreover the gradients in the meridional direction are much larger in the zonal state than in the blocked state. This means that the system will be more sensitive to barotropic instabilities. A same mechanism as in the low order model could therefore play a role in the transition to the blocked state: the system gets unstable and the perturbations on the mean flow are amplified by increasing Reynolds stresses or the presence of the topography. The mean state ($\overline{\psi_z}$) was determined as in the low order model and was defined as the mean of all the states that project into the zonal regime as it was defined by the complex network. The time averaging to calculate the TKE budgets was set to 3 days. Figure 11 shows the projection of the tendency of the TKE $\frac{\partial|\overline{\nabla\psi'|^2}}{\partial t}$ on the PC1-PC3 plane. The region associated with the ZB trajectories has increasing turbulent energy, whereas the transition from blocked to zonal is associated with decreasing turbulence.

The form drag in this model is mainly negative and acts as a sink of the energy. The values of the Reynolds stresses are positive for both the ZZ as the ZB trajectories. As the model is quite complex and the trajectories are scattered in phase space, separate trajectories do not give much insight in the dynamics of the system, as every transition seems to be associated with different values of the Reynolds stresses. Yet when the transition probability is scattered against the value of the Reynolds stresses for all the ZB trajectories, as is shown in figure 12, a positive correlation of 0.59 between those two can be found. This suggests that the Reynolds stresses are at least part of the physical mechanism of the transition and that the indicator can be interpreted as a statistical measure of those changes in the energy budget.

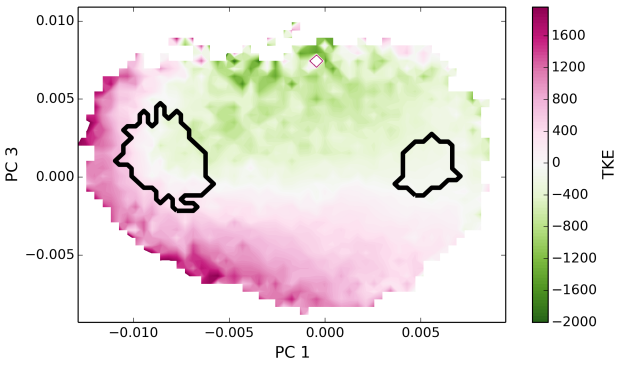

Figure 11. Projection on the PC1-PC3 plane of the tendency of TKE $\frac{\partial|\overline{\nabla\psi'|^2}}{\partial t}$. The region of the ZB trajectories is associated with an increase of turbulent energy.

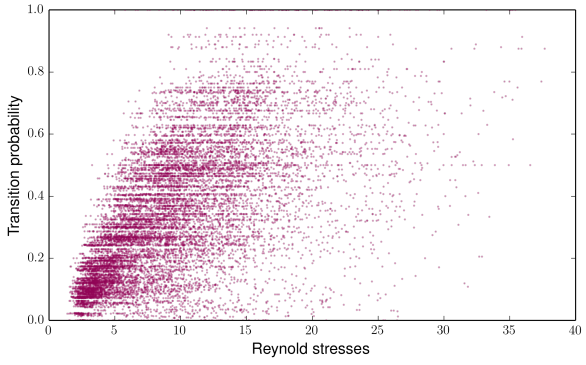

Figure 12. Scatterplot of all the ZB trajectories in the plane of the transition probability and the Reynolds stresses. The correlation is 0.59.

5 Conclusions

In this study a new method is developed to define regimes in the climate system. The method makes use of EOFs to capture the main modes of variability in the system. When the state of the climate is projected into the phase space defined by those leading modes, persistent regions or attractors can be found.

A barotropic model of the Northern Hemisphere with realistic topography and forcing is used. The bimodality in the first PC corresponds to the zonal and blocked states. When all the data are projected in the PC1-PC3 plane, a double-well potential is visible, reflecting two attracting states in the model. Those persistent regimes represent a highly attracting zonal state and a weaker attracting blocked state. During the transitions between the two states, the system has preferred directions of movement in this phase-space. By defin-

ing a complex network based on those preferred directions of movement, the attractor becomes even better visible: nodes in the attractor will be highly connected. With a community detection algorithm, the most persistent regions can be found. The pagerank of these communities was now used to define climate regimes of the system. It remains questionable what the optimal choice of this pagerank is for the definition of the regimes.

In this same PC-plane it was possible to calculate the probability of reaching the blocked regime within a certain time. This image of the evolution of the system in phase space shows the preferred pathways of the system to develop. The longer the period until the transition, the better these pathways are described. This probability-distribution can act as an indicator for the transition towards the blocked state. A warning was given when the system reached a certain probability to make the transition to the blocked state. For time lags of 40 days this resulted in 18% false alarms and 4% missed alarms. For time lags of 110 days, this was reduced to 14% and 1% respectively.

The period of prediction seems long, but the evolution of this model is much slower than it is in reality. The mean duration of the transition from the blocked to the zonal state in this model is about 60 days, and sometimes the model remains for more than 800 days in a zonal-like state. This means that a transition towards a blocked state would take almost the whole winter in the model, whereas observations show transitions on timescales of multiple days.

In the current study, the indicator was tested on the same trajectories that where used to construct the transition probability figure. It would be interesting to test if the method still applies when two separated learning and testing datasets are used. The sensitivity of the quality factor to changes in the definition of the regimes by different pakeranks was tested, but this appeared to be small.

The method provides a tool to define regimes in a highly dimensional system. With these definitions it is possible to develop a statistical method that indicates whether the system will shift into a new regime.

In a low order model it is shown that the transition from zonal to blocked flow is associated with increasing Reynolds stresses that reduce the energy of the mean state. As one of the zonal modes becomes barotropically unstable (a Hopf bifurcation in the zonal state of the model), the perturbations grow due to the increasing Reynolds stresses and perturb the other modes due to the coupling terms. During the transition, energy of the perturbations in the zonal modes is via the coupling with the topography transferred towards the meandering modes.The system gets into a state of reduced zonal strength. From there it turns slowly back to the zonal regime due to the zonal forcing.

The findings in this low order model could be applied to the T21 model to find a physical explanation of the transition in this model. As this system is much more complex, and not as symmetrical as the low order model, other processes could also be important. For example, the form drag in this model is most of the time non-zero. The topography can therefore have a (de)stabilising effect on the flow, thereby influencing the barotropic instabilities.

When the development of the TKE is plotted in the PC1-PC3 plane, a pattern becomes visible of increasing turbulence in the region of transition towards the blocked state. The region of transition to the zonal state has on average decreasing turbulence. Furthermore, a correlation is found between the Reynolds stresses and the probability of transition for the ZB trajectories. Increasing Reynolds stresses go with increased probability to make the transition. It is very plausible that remnants of the mechanism as it was found in the low order model applies to the T21 model as well, yet is affected by other processes such as a non-zero form drag. It can be concluded that the Reynolds stresses play an important role in the amplification of perturbations in the mean state and force the system into the transition.

Understanding the complex behaviour of higher order barotropic models remains challenging. Useful tools can be found in principal component analysis, complex networks, low order models and finally a proper physical insight. To test the developed method on real weather data is left for future research.

Acknowledgements. Dirk, voor zoveel vertrouwen alle jaren. Eddy, Wytze, Leon, Sjoerd, Lotte, Sharon en alle andere studenten van de studentenkamer van het IMAU, zonder jullie zou de studie niet een kwart zo leuk zijn geweest. Mijn ouders Geert-Jan en Caroline, voor alle vrijheid. Henk en Alexis, dank voor alle inspiratie en hulp.

References

Benilov, E. S.: The Stability of Zonal Jets in a Rough-Bottomed Ocean on the Barotropic Beta Plane, Journal of Physical Oceanography, 30, 733–740, doi:10.1175/1520-0485(2000)030<0733:TSOZJI>2.0.CO;2, http://journals.ametsoc.org/doi/abs/10.1175/1520-0485%282000%29030%3C0733%3ATSOZJI%3E2.0.CO%3B2, 2000.

Benilov, E. S., Nycander, J., and Dritschel, D. G.: Destabilization of barotropic flows small-scale topography, Journal of Fluid Mechanics, 517, 359–374, doi:10.1017/S0022112004000990, http://www.journals.cambridge.org/abstract_S0022112004000990, 2004.

Brin, S. and Page, L.: The anatomy of a large-scale hypertextual Web search engine, Computer Networks and ISDN Systems, 30, 107–117, doi:10.1016/S0169-7552(98)00110-X, http://linkinghub.elsevier.com/retrieve/pii/S016975529800110X, 1998.

Charney, J. and DeVore, J.: Multiple flow equilibria in the atmosphere and blocking, Journal of the atmospheric sciences, 36, 1205–1216, papers://afd69f4a-9dc5-41a6-8e4b-3b88c5de2ef8/Paper/p77, 1979.

Croci-Maspoli, M., Schwierz, C., and Davies, H. C.: Atmospheric blocking: space-time links to the NAO and PNA, Climate Dy-

namics, 29, 713–725, doi:10.1007/s00382-007-0259-4, http://link.springer.com/10.1007/s00382-007-0259-4, 2007.

Crommelin, D.: Regime Transitions and Heteroclinic Connections in a Barotropic Atmosphere, Journal of Atmospheric Sciences, 60, 229–246, 2003.

Crommelin, D., Opstelten, J., and Verhulst, F.: A Mechanism for Atmospheric Regime Behavior, Journal of Atmospheric Sciences, 61, 1406–1419, 2004.

de Swart, H. E.: Analysis of a six-component atmospheric spectral model: chaos, predictability and vacillation, Physica D, 36, 222–234, papers://afd69f4a-9dc5-41a6-8e4b-3b88c5de2ef8/Paper/p139, 1989.

Dijkstra, H.: The North Atlantic Oscillation, in: Nonlinear climate dynamics, pp. 131–167, Cambridge University Press, papers://afd69f4a-9dc5-41a6-8e4b-3b88c5de2ef8/Paper/p31, 2013.

Frederiksen, C. and Frederiksen, J. S.: Flow over topography and instability on beta-planes: the effects of different expansion representations, Journal of Atmospheric Sciences, 46, 1664 – 1686, 1989.

Frederiksen, C. and Frederiksen, J. S.: Flow over topography and instability on a sphere, Journal of the Atmospheric Sciences, 48, 2411 – 2425, 1991.

Holloway, G.: Systematic forcing of large-scale geophysical flows by eddy-topography interaction, Journal of Fluid Mechanics, 184, 463–476, doi:10.1017/S0022112087002970, http://www.journals.cambridge.org/abstract_S0022112087002970, 1987.

Itoh, H. and Kimoto, M.: Multiple Attractors and Chaotic Itinerancy in a Quasigeostrophic Model with Realistic Topography: Implications for Weather Regimes and Low-Frequency Variability, Journal of Atmospheric Sciences, 53, 2217–2231, 1996.

Jin, F.-F. and Ghil, M.: Intraseasonal Oscillations in the Extratropics: Hopf Bifurcation and Topographic Instabilities, Journal of Atmospheric Sciences, 47, 3002–3022, 1990.

Kuznetsov, Y. A., Muratori, S., and Rinaldi, S.: Homoclinic bifurcations in slow-fast second order systems, Nonlinear analysis, methods and applications, 25, 747–762, papers://afd69f4a-9dc5-41a6-8e4b-3b88c5de2ef8/Paper/p138, 2004.

Legras, B. and Ghil, M.: Persistent Anomalies, Blocking and Variations in Atmospheric Predictability, Journal of Atmospheric Sciences, 42, 433–471, 1985.

Lejenäs, H. and Ø kland, H.: Characteristics of northern hemisphere blocking as determined from a long time series of observational data, Tellus A, 35A, 350–362, doi:10.1111/j.1600-0870.1983.tb00210.x, http://tellusa.net/index.php/tellusa/article/view/11446, 1983.

Lenton, T.: Early warning of climate tipping points, Nature Publishing Group, 1, 201–209, http://dx.doi.org/10.1038/nclimate1143papers://afd69f4a-9dc5-41a6-8e4b-3b88c5de2ef8/Paper/p25, 2011.

Mauritsen, T. and Källén, E.: Blocking prediction in an ensemble forecasting system, Tellus, 56A, 218–228, 2004.

Newman, M. E. J. and Girvan, M.: Finding and evaluating community structure in networks, pp. 1–16, papers://afd69f4a-9dc5-41a6-8e4b-3b88c5de2ef8/Paper/p146, 2008.

Pelly and Hoskins: A new perspective on blocking, Journal of Atmospheric Sciences, 60, 743–754, papers://afd69f4a-9dc5-41a6-8e4b-3b88c5de2ef8/Paper/p27, 2003.

Rex, D.: Blocking Action in the Middle Troposphere and its Effect upon Regional Climate. I., Tellus, 2, 196–211, 1950a.

Rex, D.: Blocking Action in the Middle Troposphere and its Effect upon Regional Climate. II., Tellus, 2, 275–301, 1950b.

Rosvall, M. and Bergstrom, C. T.: Maps of random walks on complex networks reveal community structure, PNAS, 105, 1118–1123, papers://afd69f4a-9dc5-41a6-8e4b-3b88c5de2ef8/Paper/p150, 2008.

Rosvall, M. and Bergstrom, C. T.: Multilevel compression of random walks on networks reveals hierarchical organization in large integrated sys, pp. 1–11, papers://afd69f4a-9dc5-41a6-8e4b-3b88c5de2ef8/Paper/p152, 2011.

Scheffer, M., Bascompte, J., Brock, W. a., Brovkin, V., Carpenter, S. R., Dakos, V., Held, H., van Nes, E. H., Rietkerk, M., and Sugihara, G.: Early-warning signals for critical transitions., Nature, 461, 53–9, doi:10.1038/nature08227, http://www.ncbi.nlm.nih.gov/pubmed/19727193, 2009.

Selten, F. M.: An efficient description of the dynamics of the barotropic flow, Journal of Atmospheric Sciences, 52, 915–936, papers://afd69f4a-9dc5-41a6-8e4b-3b88c5de2ef8/Paper/p129, 1995.

Thompson, D. W. and Wallace, J. M.: Regional climate impacts of the Northern Hemisphere annular mode., Science (New York, N.Y.), 293, 85–9, doi:10.1126/science.1058958, http://www.ncbi.nlm.nih.gov/pubmed/11441178, 2001.

Tibaldi, S. and Molteni, F.: On the operational predictability of blocking, Tellus, 42A, 343–365, 1990.

Viebahn, J. and Dijkstra, H. a.: Critical Transition Analysis of the Deterministic Wind-Driven Ocean Circulation - A Flux-Based Network Approach, International Journal of Bifurcation and Chaos, 24, 1430 007:1–32, doi:10.1142/S0218127414300079, http://www.worldscientific.com/doi/abs/10.1142/S0218127414300079, 2013.

Warren, B., LaCasce, J., and Robbins, P.: On the obscurantist physics of 'Form Drag' in theorizing about the circumpolar current, Journal of Physical Oceanography, 26, 2297–2301, 1996.

Woollings, T., Hoskins, B., Blackburn, M., and Berrisford, P.: A New Rossby Wave–Breaking Interpretation of the North Atlantic Oscillation, Journal of the Atmospheric Sciences, 65, 609–626, doi:10.1175/2007JAS2347.1, http://journals.ametsoc.org/doi/abs/10.1175/2007JAS2347.1, 2008.